



Experimental Phase Functions of Millimeter-sized Cosmic Dust Grains

O. Muñoz¹, F. Moreno¹, F. Vargas-Martín², D. Guirado¹, J. Escobar-Cerezo¹, M. Min^{3,4}, and J. W. Hovenier⁴

¹Instituto de Astrofísica de Andalucía, CSIC, Glorieta de la Astronomía s/n, E-18008 Granada, Spain

²Department of Electromagnetism and Electronics, University of Murcia, E-30100 Murcia, Spain

³SRON Netherlands Institute for Space Research, Sobornnelaan 2, 3584 CA Utrecht, The Netherlands

⁴Astronomical Institute “Anton Pannekoek,” University of Amsterdam, Science Park 904, 1098 XH, Amsterdam, The Netherlands

Received 2017 April 17; revised 2017 July 12; accepted 2017 July 12; published 2017 September 1

Abstract

We present the experimental phase functions of three types of millimeter-sized dust grains consisting of enstatite, quartz, and volcanic material from Mount Etna, respectively. The three grains present similar sizes but different absorbing properties. The measurements are performed at 527 nm covering the scattering angle range from 3° to 170°. The measured phase functions show two well-defined regions: (i) soft forward peaks and (ii) a continuous increase with the scattering angle at side- and back-scattering regions. This behavior at side- and back-scattering regions is in agreement with the observed phase functions of the Fomalhaut and HR 4796A dust rings. Further computations and measurements (including polarization) for millimeter-sized grains are needed to draw some conclusions about the fluffy or compact structure of the dust grains.

Key words: comets: general – dust, extinction – protoplanetary disks – scattering

1. Introduction

Small dust particles are ubiquitous in many different astrophysical bodies ranging from planetary and cometary atmospheres, zodiacal clouds, and planetary rings to debris disks and protoplanetary systems. The way those small particles scatter and absorb stellar light affects the thermal structure of the body under study and, subsequently, its chemical and dynamical properties. The spectral dependence of light scattered by those particles is widely used for retrieving the physical properties of the grains and their spatial distribution.

Dust grains in planetary atmospheres (Rages & Pollack 1983; Tomasko et al. 1999; Wolff et al. 2010), debris, and protoplanetary disks (Weinberger et al. 1999) usually produce strong forward scattering and nearly a flat dependence of the scattering angle at side- and back-scattering regions. This seems to indicate the presence of compact and/or aggregate dust grains with sizes ranging from sub-micron up to tens of microns. Those findings are in agreement with laboratory measurements of cosmic dust analogs (Volten et al. 2006, 2007; Laan et al. 2009; Muñoz et al. 2012; Dabrowska et al. 2015).

There are some astronomical observations that indicate the presence of millimeter-sized cosmic dust grains. Such is the case of comet 67P/Churyumov–Gerasimenko, the target of the ESA *Rosetta* mission. The main conclusions from the Grain Impact Analyser and Dust Accumulator (GIADA) instrument provide a scenario in which we can find compact particles with sizes ranging from 0.03 mm up to 1 mm and fluffy aggregates from sub-micron up to 2.5 mm (Fulle et al. 2015). Moreover, preperihelion observations of the Optical, Spectroscopic, and Infrared Remote Imaging System (OSIRIS) cameras indicate that dust optical scattering is dominated by 100 μm to millimeter-sized grains (Rotundi et al. 2015).

Apart from comets, circumstellar disks also can host large cosmic dust grains (e.g., Andrews & Williams 2005; Canovas et al. 2015, 2016; Kataoka et al. 2016). Interesting case studies related to circumstellar disks are reported by Kalas et al. (2005) and Milli et al. (2017) for dust orbiting Fomalhaut and HR

4796A, respectively. *HST* imaging of Fomalhaut shows that a very small fraction of the stellar light is scattered into our line of sight. Moreover, the phase function at side- and back-scattering regions increases with the scattering angle (Le Bouquin et al. 2009). A similar behavior has been recently reported by Milli et al. (2017) for the HR 4796A dust ring. This scattering behavior could be caused by the presence of large grains; $r \geq 100 \mu\text{m}$ in the Fomalhaut and $r \sim 30 \mu\text{m}$ in the HR 4796A dust rings, respectively (Min et al. 2010; Milli et al. 2017). A subsequent analysis of far-infrared images of Fomalhaut obtained with the *Herschel Space Observatory* (Acke et al. 2012) indicates that the belt around Fomalhaut could consist of fluffy aggregates. The main reason is that large compact grains do not have the thermal properties needed to explain the far-infrared images. On the contrary, fluffy aggregates consisting of small monomers could have the absorption properties of small grains, showing the scattering anisotropy of large particles. Still, simulated phase functions of fractal aggregates (e.g., Bertini et al. 2007; Mischenko & Liu 2007; Moreno et al. 2007; Okada et al. 2008; Min et al. 2016) and experimental phase functions of aggregates with sizes larger than the wavelength of the incident light (Volten et al. 2007) provide a strong diffraction spike but do not reproduce the observed slope of the phase function at side- and back-scattering angles. We might note that numerical scattering simulations of fractal aggregates are limited to sizes of the order of or slightly larger than the wavelength of the incident light. Therefore, the solution of the problem remains unclear.

Those are examples that illustrate that the retrieval of the physical characteristics of cosmic dust grains from the observed scattered light is far from trivial. If the dust cloud of interest consists of spherical particles we can perform computations without any restriction about the size or composition by means of the Lorenz–Mie theory (van de Hulst 1957). However, the scattering properties of irregular cosmic dust grains can differ dramatically from those of equivalent spheres. Due to their complicated morphology in most cases, computations for polydisperse cosmic dust grains have to be replaced by simplified models such as spheroids (Kim & Martin 1995; Mishchenko et al. 1997) or hollow spheres (Min et al. 2005).

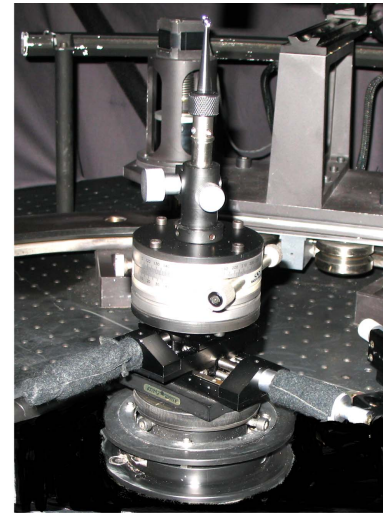
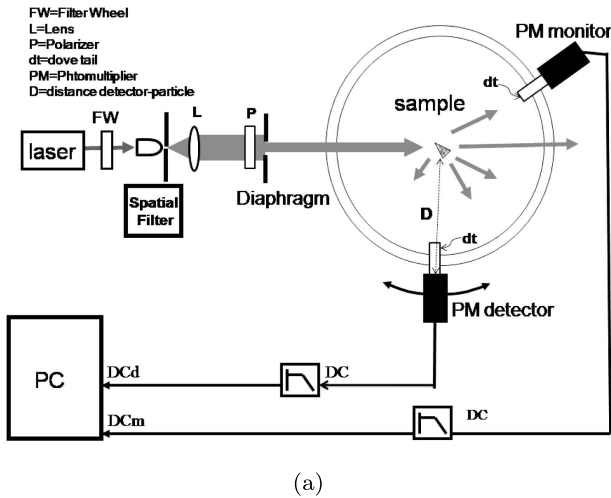


Figure 1. (a) Schematic overview of the experimental light scattering apparatus as seen from above. (b) Photograph of the flat black holder mounted on the x - y rotating table. The N-BK7 glass sphere is located on its conical tip.

Experimental data should then be used to validate the computational results. Computations for dust grains of arbitrary shapes are more complicated and limited to particles with sizes comparable to the wavelength (Mackowski & Mishechenko 2011). Thus, controlled laboratory experiments of light scattering by cosmic dust grains covering different size ranges, shapes, and compositions remain as indispensable tools to study the scattering behavior of the irregular dust grains.

In this work we present the measured phase functions for three different types of millimeter-sized cosmic dust grains analogs. This size range is still poorly studied due to the limitations of the numerical codes and technical difficulties related to the experiments. The paper is organized as follows. In Section 2 we summarize the main concepts of light scattering, providing a description of the experimental apparatus in Section 3. Test measurements regarding the reliability of the experimental data are presented in Section 4. In Sections 5 and 6, we describe the physical characteristics of the dust grains and experimental phase functions, respectively. Finally, we summarize our results in Section 7.

2. The Scattering Matrix Formalism

The flux vector of the light scattered by one particle in a particular orientation, p , is related to the flux vector of the incident beam, $\pi\Phi_0$, by means of the scattering matrix, F^p , as (Hovenier et al. 2004)

$$\Phi_{\text{det}} = \frac{\lambda^2}{4\pi^2 D^2} F^p \Phi_0, \quad (1)$$

where λ is the wavelength and D is the distance between the particle and the detector. Here, $\pi\Phi_{\text{det}}$ is the flux vector at the detector and F^p is the scattering matrix of the particle in a particular orientation. All elements of F^p are dimensionless and depend on the physical properties of the particle (size, shape, porosity, surface roughness, and refractive index), and the direction of scattering, i.e., the direction from the particle to the detector. The direction of scattering is defined by the scattering angle, θ , the angle between the directions of propagation of the incident and the scattered beams ($0 \leq \theta \leq \pi$), and an azimuth

angle, ϕ , that ranges from 0 to 2π . In general, F^p contains 16 nonvanishing elements:

$$F^p = \begin{pmatrix} F_{11}^p & F_{12}^p & F_{13}^p & F_{14}^p \\ F_{21}^p & F_{22}^p & F_{23}^p & F_{24}^p \\ F_{31}^p & F_{32}^p & F_{33}^p & F_{34}^p \\ F_{41}^p & F_{42}^p & F_{43}^p & F_{44}^p \end{pmatrix}. \quad (2)$$

In the case of a particle in random orientation, all scattering planes are equivalent. Thus, the scattering direction is fully described by the scattering angle θ . Further, for a homogeneous sphere the scattering matrix has only four independent elements that are not identically equal to zero, i.e., it has the form

$$F^p = \begin{pmatrix} F_{11}^p & F_{12}^p & 0 & 0 \\ F_{12}^p & F_{11}^p & 0 & 0 \\ 0 & 0 & F_{33}^p & F_{34}^p \\ 0 & 0 & -F_{34}^p & F_{33}^p \end{pmatrix}. \quad (3)$$

For unpolarized incident light, the first element of the scattering matrix, $F_{11}^p(\theta)$, is proportional to the flux of the scattered light and is called the phase function or the scattering function.

3. Experimental Apparatus

The light scattering measurements have been performed at the IAA cosmic dust laboratory (Muñoz et al. 2010, 2011). In this work, the experimental apparatus has been adapted to measure the angular dependence of the flux scattered by a single particle with a size much larger than the wavelength of the incident light. A schematic overview of the experimental apparatus is presented in Figure 1(a). We use a linearly polarized continuous-wave tunable Argon-Krypton laser tuned at 520 nm. A spatial filter has been used to avoid spatial intensity variations in the laser beam. In this way we assure a homogeneous illumination over the entire particle. The homogeneous beam is collimated by a lens before passing through a polarizer, P , oriented at 45° . The polarized beam is scattered by the particle of interest. This is located on a 2 mm

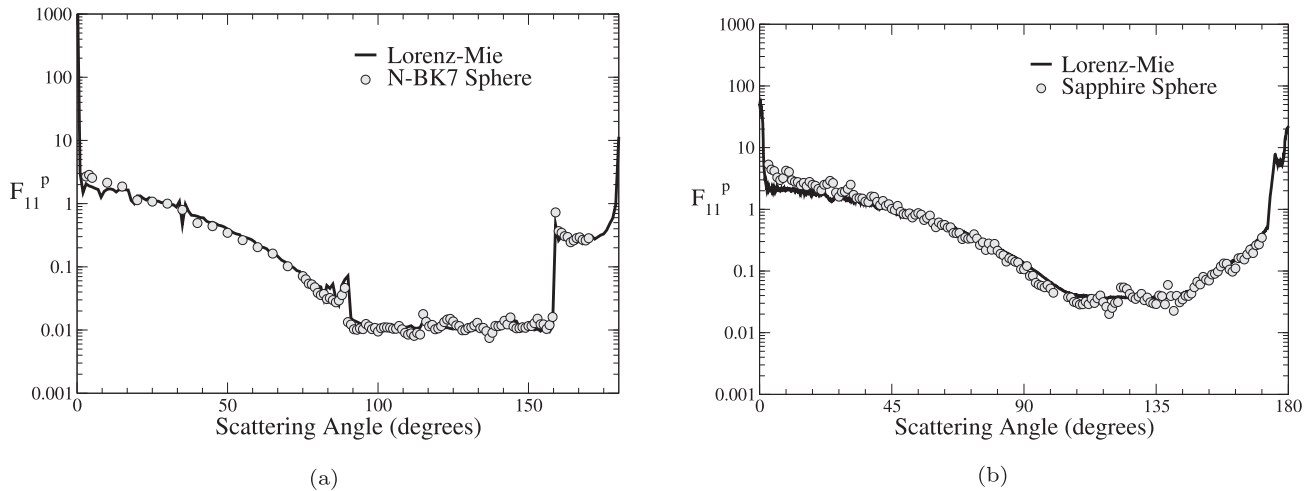


Figure 2. Comparison of phase functions based on the measured data and the Lorenz–Mie computations (solid black) for the N-BK7 (a) and Sapphire (b) calibration spheres (gray circles).

Table 1
Properties of the Calibration Spheres and Cosmic Dust Grains

Composition	Diameter (mm)	$m = n+ki$ (520 nm)	
N-BK7	5.0	1.5168+9E-9i	Edmund Optics Catalog
Sapphire	5.0	1.77+0i	Edmund Optics Catalog
Enstatite	6.4 ^a	1.58+2E-05i	Dorschner et al. (1995)
Quartz	7.8 ^a	1.54+0i	Klein & Hurbulst (1993)
Etna	7.0 ^a	1.59+0.01i	Ball et al. (2015)

Note.

^a Diameter of the volume-equivalent sphere.

conical-tip flat black holder mounted on a x – y rotating table (Figure 1(b)). A filter wheel equipped with gray filters of different densities is located between the laser and spatial filter. It is operated from the computer so that the flux of the incident beam can be scaled to its most appropriate value for each scattering angle. The unscattered part of the incident beam is absorbed by a beam-stop. Moreover, we use a diaphragm behind the polarizer, P , to control the width of the beam so that only the particle of interest is illuminated and not the holder. The scattered light is detected by a photomultiplier tube (the detector: 9828A Electron tubes). Another photomultiplier tube (the monitor) is located at a fixed position and is used to correct for fluctuations in the laser beam. Both photomultipliers are positioned on a ring with an outer diameter of one meter. The detector and monitor are mounted on dove tails (dt) so that they can be moved forward and backward. In this case the detector is located at a distance, D , of 62 cm to the particle. The detector moves along the ring in steps of 5° , 1° , or even smaller if a higher angular resolution is required, covering a scattering angle range from 3° (nearly forward scattering) to 170° (nearly backward scattering).

4. Test Measurements

The reliability of the measurements is tested by comparing the measured phase function of two calibration spheres to the results of the Lorenz–Mie calculations for the corresponding size and refractive index. Physical properties of the N-BK7 glass and Sapphire spheres (Edmund Optics) are presented in

Table 1. The size of the calibration spheres has been chosen similar to that of our particles of interest.

In Figures 2(a) and (b), we present the measured and calculated phase functions as functions of the scattering angle for the N-BK7 and Sapphire calibration spheres, respectively. The measured and calculated $F_{11}^P(\theta)$ are plotted on a logarithmic scale and normalized to 1 at 30° . During the test measurements, the detector is moved along the ring in steps of 1° . The plotted values corresponding to the Lorenz–Mie calculations are averaged over $\pm 0.25^\circ$ according to the angular resolution of the experimental setup. As shown in Figures 2(a) and (b), the measured phase functions show an excellent agreement with the Lorenz–Mie computations over the entire angle range. Small differences might be caused by small inhomogeneities in the calibration sphere. Moreover, the measured results are strongly dependent on the exact position of the calibration sphere at the center of the measuring ring.

5. Dust Grains

In this work we study three types of millimeter-sized grains consisting of enstatite, quartz, and volcanic material from Mount Etna, respectively. The three grains have been chosen so that they would have similar sizes but different absorbing properties. Mount Etna is a quite dark material, whereas Enstatite and Quartz present a nearly zero imaginary part of the refractive index at the studied wavelength (527 nm). In this way we can study how absorption affects the measured phase functions. Their physical properties are summarized in Table 1. Moreover, all dust grains present similar sizes as the BK7 and Sapphire

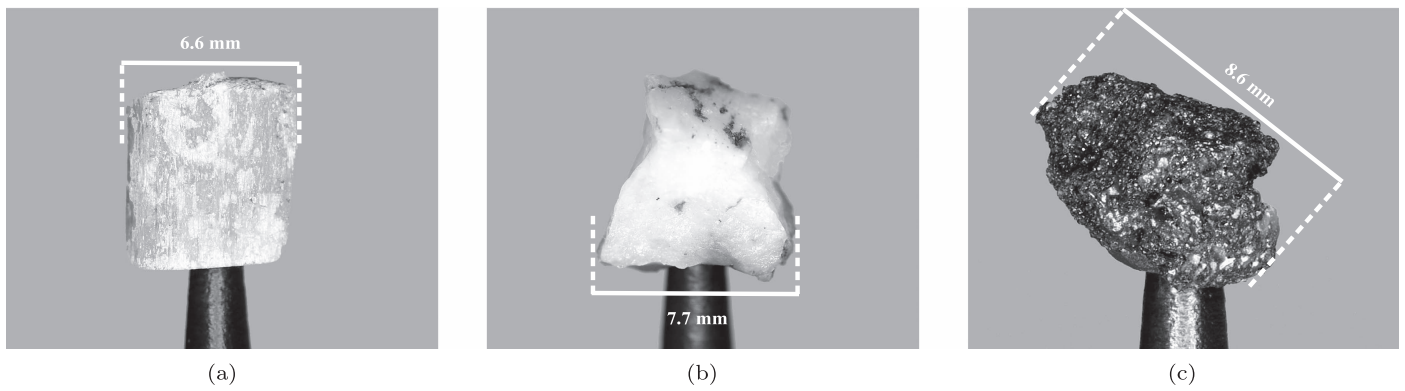


Figure 3. Optical images of enstatite (a), quartz (b), and Etna (c) grains.

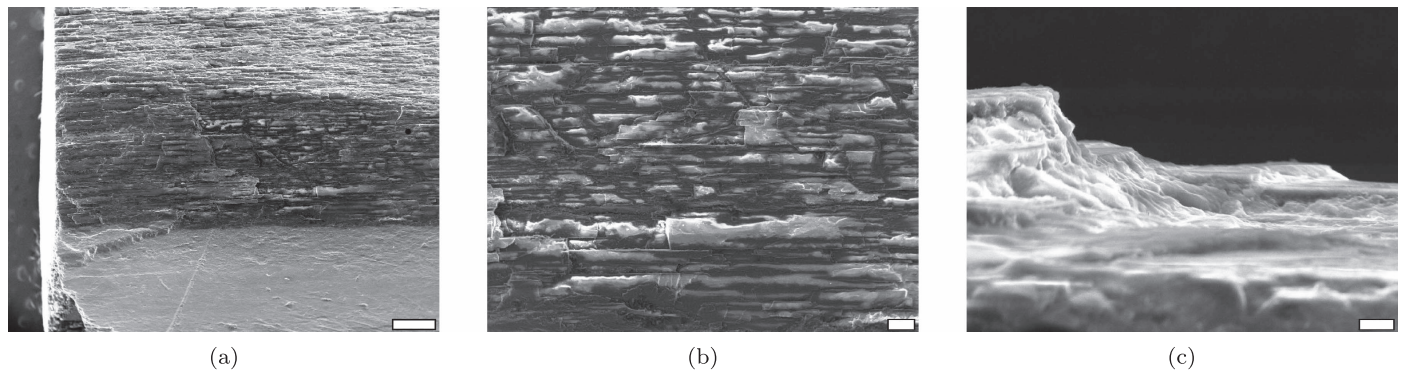


Figure 4. Scanning electronic microscope images of enstatite. The white bars denote 500 μm (a), 100 μm (b), and 10 μm (c), respectively.

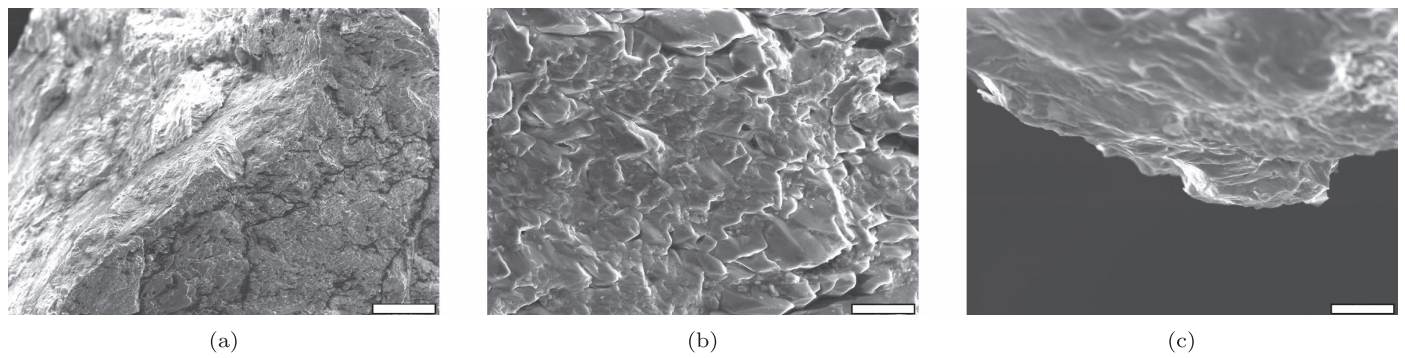


Figure 5. Scanning electronic microscope images of quartz. The white bars denote 500 μm (a), and 50 μm , and (b) and (c), respectively.

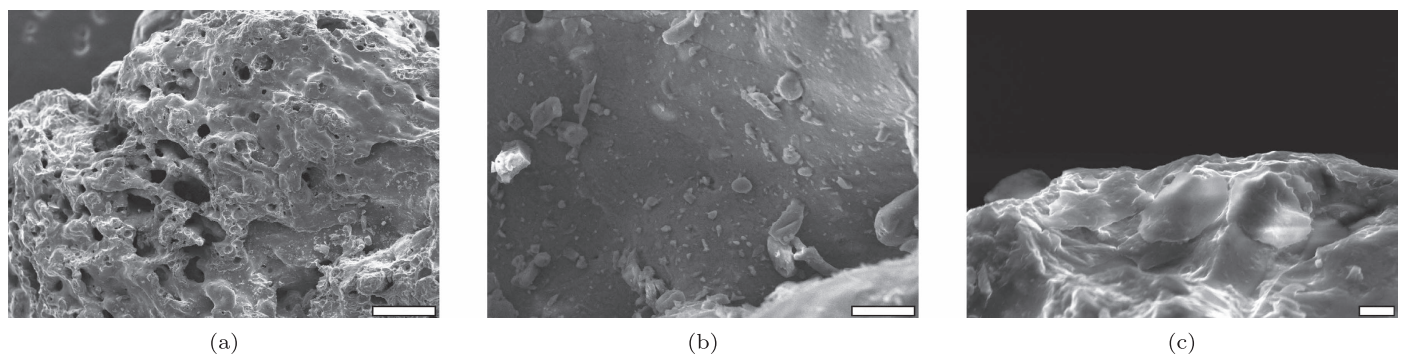


Figure 6. Scanning electronic microscope images of the Etna grain. The white bars denote 500 μm (a), 50 μm (b), and 10 μm (c), respectively.

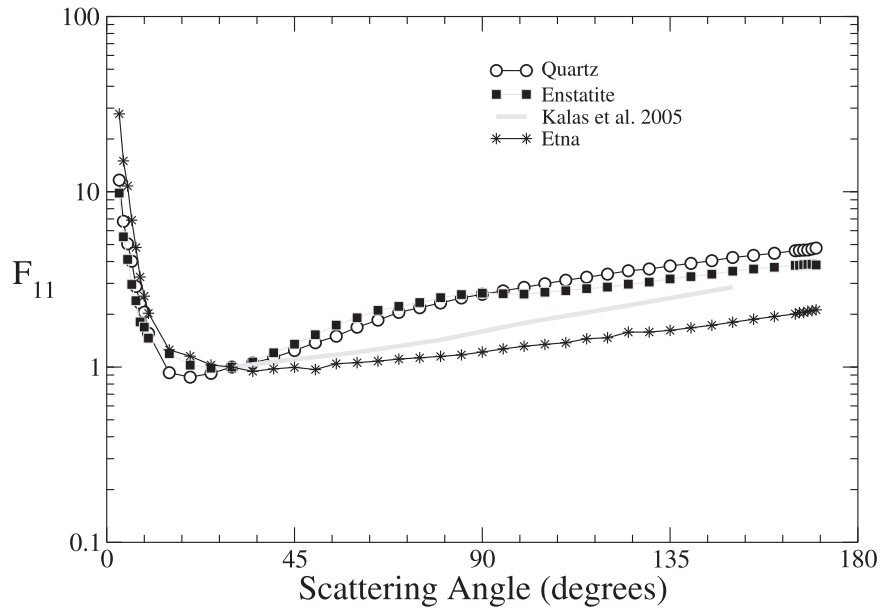


Figure 7. Experimental phase functions at 520 nm for quartz (filled circles), enstatite (filled squares), and Etna (triangles). The observed phase function of the Fomalhaut disk grains from Kalas et al. (2005) is also shown. All phase functions are normalized to unity at 30° . Errors are indicated by error bars or are within the symbols.

spheres used to test the experimental apparatus. In this way we assure a homogeneous illumination over the entire grain.

In Figure 3 we present optical images of the three dust grains. It is interesting to note that even in the optical images we can distinguish surface roughness. This is the case particularly of the Etna grain, which presents the typical structure of vesicular volcanic grains composed of porous material and cratered surfaces (Riley et al. 2003). The vesicular structure is produced by gas bubbles that escape when the volcanic melt is cooled to glass. To estimate the scale of the surface roughness of our dust grains in Figures 4–6, we present scanning electronic microscope images. As shown the three studied grains present not only intrinsic surface roughness with sizes of the order of or smaller than the wavelength of the incident light, but also micron-sized grains that might affect their optical properties (Figures 4–6, top right panels).

6. Results and Discussion

In Figure 7 we present the measured phase functions for the enstatite, Etna and quartz dust grains at 520 nm. The measurements are presented together with the observed phase function of the Fomalhaut dust grains obtained with the Henyey–Greenstein parameterization retrieved by Kalas et al. (2005). The Henyey–Greenstein phase function is constrained to the observable range of the Fomalhaut system. All phase functions are normalized to unity at 30° scattering angle and are presented on a logarithmic scale.

The procedure of the measurements is as follows. The detector is moved along the ring in steps of 1° or 5° covering the scattering angle range from 3° to 170° . During the measurements the particles are located on the rotating conical holder as shown in Figure 1(b). A rigorous 3D-orientation average could be obtained by a sufficient number of Euler rotations: (i) rotation around the vertical axis, α ; (ii) rotation around the direction of the laser beam, β ; and (iii) rotation around the axis perpendicular to the base of the particle, γ . For

an optimal performance, α and γ should be uniformly distributed, while β ought to follow a distribution proportional to $\sin(\beta)$ (Mishchenko & Yurkin 2017). Such a procedure would require a holder with two degrees of freedom that would significantly complicate the performance of the measurements. Instead, we have assumed a 1-axis orientation average as an approximate solution. This is equivalent to a 3D-orientation average in the case that the revolution volume of the particle is symmetrical in regard to the scattering plane. This condition is fulfilled up to a high degree by our cosmic grains as shown in Figure 3. Thus, to simulate random orientation the plotted figures, $F_{11}(\theta)$, are the results of averaging over 36 $F_{11}^p(\theta)$, corresponding to 36 different orientations. Starting with a given orientation, a particle is measured after each of the 36 successive rotations of 10° . We assume that the number of orientations is sufficient when adding more orientations of the particle on the vertical axis (perpendicular to the direction of the detector) does not affect the final result. Special tests are performed to verify that other directions are irrelevant for such irregular grains. In those tests the position of the grain on the holder is rotated 90° about a horizontal plane. Starting from a given position, the grain was measured after each of the two 90° rotations about the vertical axis. It is verified that adding those extra orientations does not affect the final result. In conclusion, taking into account the orientation over the horizontal axis plays no significant role in our experimental results. That is a good indication that the measurements can be considered in random orientation even though, strictly speaking, the phase function has not been averaged over all possible orientations.

In all three measured phase functions we can distinguish two well-defined regions. In the first region, soft forward peaks in the 3° to $\sim 20^\circ$. In the second region, in the scattering angle range from $\sim 20^\circ$ to 170° , the three phase functions increase with the scattering angle. This increase is stronger in the case of the two non-absorbing grains, enstatite and quartz. For the sizes of our dust grains, the ray optics approximation can be used. It

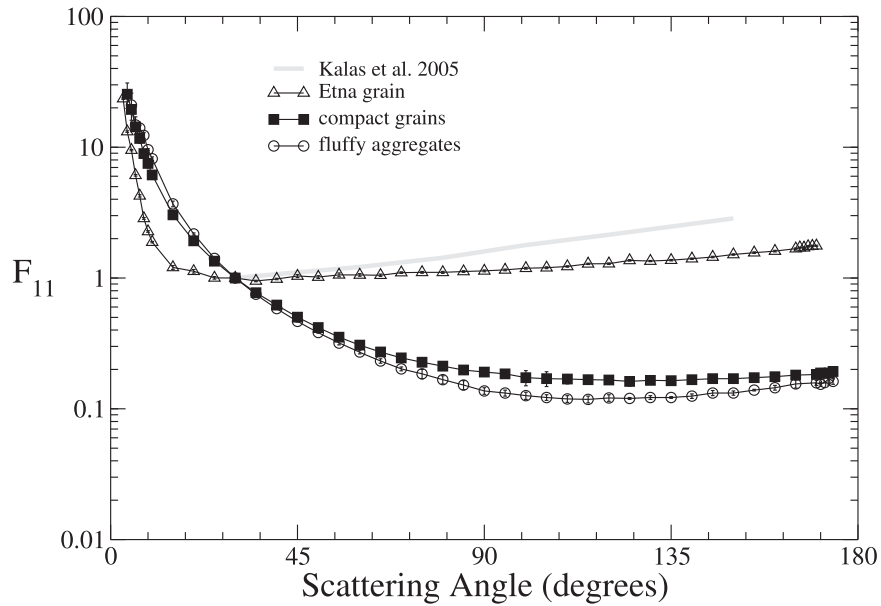


Figure 8. Experimental phase functions for the Etna dust grain ($r = 3.5$ mm; triangles), compact particles ($r_{\text{eff}} = 124.75$ μm ; Muñoz et al. 2007), and micron-sized fluffy aggregates (circles; Volten et al. 2006). The observed phase function of the Fomalhaut disk grains from Kalas et al. (2005) is also shown. All phase functions are normalized to unity at 30° . Errors are indicated by error bars or are within the symbols.

is based on the assumption that the incident plane wave can be represented as a collection of independent parallel rays. The rays hitting the particle result in two phenomena: (i) diffraction that is constrained into a narrow intensive lobe around the exact forward direction (0°), and (ii) reflection and refraction that contribute to the total scattering by the particle (van de Hulst 1957).

The angular width of the diffraction peak for the size of our dust grains and distance to the detector, D , is of the order of $\pm 0.8^\circ$ around the exact forward direction that is beyond the measurable angle range of our experiment. Therefore, diffraction by the large grains cannot be responsible for the measured forward peaks.

It is known that wavelength-scale surface roughness can significantly affect the scattering properties of dust grains (Muñoz et al. 2007; Nousiainen et al. 2011; Lindqvist et al. 2011; Escobar-Cerezo et al. 2017). As presented in Figures 4–6 our particles are covered not only by various types of surface structures and cavities, but also by small particles. Therefore, the measured forward peaks in the 3° to $\sim 20^\circ$ scattering angle range might be due to scattering by the wavelength-scale surface roughness and surface micron-sized particles of our grains.

As mentioned, at side- and back-scattering regions all measured $F_{11}(\theta)$ increase with the scattering angle. In the case of the Etna grain, that presents a high imaginary part of the refractive index, the transmitted part can be ignored and therefore the measured phase function in the $\sim 20^\circ$ – 170° region might be due to reflexion on the surface of the particle. That is not the case for the enstatite and quartz grains in which refracted light, after another refraction, may emerge from the particle, contributing to the measured intensity at side- and back-scattering regions producing the measured higher slope of $F_{11}(\theta)$ in the mentioned region.

As shown in Figure 7, the empirical phase function of the grains orbiting Fomalhaut lies within the domains occupied by the measured phase functions for the millimeter-sized non-absorbing

and highly absorbing dust grains, respectively. That seems to indicate that the Fomalhaut dust ring could be dominated by very large grains.

Several model particles have been suggested to reproduce the *HST* optical and/or *Herschel* far-infrared images of the Fomalhaut system. Dust grains should be large enough so that the diffraction spike is narrowly forward peaked and therefore outside of the observable angle range. The analysis of *HST* optical images performed by Min et al. (2010) establishes a lower limit diameter of 100 μm for the grains in the Fomalhaut dust ring. Further studies including an analysis of *Herschel* far-infrared images add another constraint to the dust grains populating the disk. They should simultaneously scatter light like large grains and absorb and emit like small grains. That calls for more sophisticated model particles such as fluffy aggregates (Acke et al. 2012) that, in principle, could fulfill both of the conditions. In Figure 8 we present the experimental phase functions for three different samples of cosmic dust analogs, namely, a size distribution of silicate-type compact particles (Muñoz et al. 2007), a size distribution of fluffy aggregates (Volten et al. 2007), and the Etna grain presented in this work. The experimental data are presented together with the retrieved phase function for the Fomalhaut disk grains. The compact sample consists of silicate dust particles collected in the Sahara desert (Libya). Its refractive index at the measurement wavelength (632.8 nm) is equal to $m = 1.5 + i0.0004$, similar to that found in enstatite, an iron-free pyroxene (Dorschner et al. 1995). Its effective radius, r_{eff} , and variance, v_{eff} , are equal to 125 μm and 0.15 , respectively. Therefore, the dust grains of this sample show sizes larger than that of the lower limit established by Min et al. (2010). Further details can be found in Muñoz et al. (2007).

The aggregate sample was produced in a condensation flow apparatus in an experiment intended to mimic the formation of circumstellar dust. The phase function presented in Figure 8 corresponds to a magnesian silicate sample labeled as Aggregate1 in Volten et al. (2007). The measurements are performed at

632.8 nm. The aggregate size is estimated to be of the order of 20 μm with modal grain sizes ranging from 50 to 120 nm depending on its composition, i.e., it consists of aggregates with sizes similar to those estimated for the grains populating the HR 4796A dust ring. A detailed description of the sample is provided in Volten et al. (2007). The measured phase function for the compact and aggregate samples are freely available in the Amsterdam–Granada light scattering database (<http://www.iaa.es/scattering>) under request of citation of Muñoz et al. (2012) and the paper in which the data were published.

As shown in Figure 8, both the compact and aggregate samples produce a narrow diffraction spike compatible with the *HST* Fomalhaut images. However, in both cases the measured phase functions decrease at side-scattering angles showing a nearly flat dependence in the scattering angle range from 90° to 177° . This seems to be a general trend for irregular dust particles with sizes ranging from sub-micron up to a hundred microns (Muñoz et al. 2012). That behavior does not agree with the observed slope of the phase function for Fomalhaut and HR 4796A grains. On the contrary, the phase function for the millimeter-sized Etna grain shows a nearly perfect fit to the observations. That seems to support the hypothesis that the Fomalhaut and HR 4796A dust rings could be dominated by dust grains that are significantly larger than a hundred microns. In the case of Fomalhaut, those large grains should present a fractal structure to mimic the observed far-infrared spectra. However, it is not clear yet if such large aggregates can reproduce the observed phase function. Unfortunately, computations for aggregates are limited to sizes significantly smaller than the size of the grains expected to be in protoplanetary and debris disks as the finding of the *Rosetta* mission indicate (e.g., Fulle et al. 2015; Rotundi et al. 2015; Hilchenbach et al. 2016; Mannel et al. 2016). Even with ever-increasing algorithms sophistication, light scattering computations for dust grains of arbitrary shapes are still limited to particles with sizes comparable to the wavelength (Mackwoski & Mishechenko 2011). Thus, further experimental phase functions of millimeter-sized aggregates consisting of micron-sized monomers are needed to know if such large aggregates could produce the observed slopes of the phase functions in the Fomalhaut and HR 4796A dust rings.

7. Conclusions

We present the experimental phase function of three millimeter-sized cosmic dust analogs. The measurements are performed at 520 nm covering the scattering angle range from 3° to 170° . The reliability of the experimental apparatus has been tested by the comparison of the measured phase function of two calibration spheres from Edmund Optics with Lorenz–Mie computations for the corresponding size and refractive index. The three studied grains consist of enstatite, quartz, and volcanic material from Mount Etna. In all studied cases the measured phase functions show two well-defined regions: (i) a soft forward peak and (ii) a continuous increase with the scattering angle at side- and back-scattering regions. That increase is stronger in the case of the non-absorbing grains, namely, enstatite and quartz.

Experimental data presented in this work indicate that the scattering in the disk around Fomalhaut and HR 4796A could be dominated by large irregular cosmic dust grains. In the case of Fomalhaut, the combination of this conclusion with that based on the analysis of the far-infrared spectra, as reported by

Acke et al. (2012), would drive us to a model of dust grains consisting of fractal aggregates with sizes significantly larger than the wavelength of the incident light. Such large particles are in agreement with last findings obtained for comet 67P/Churyumov–Gerasimenko, the target of the ESA *Rosetta* mission (e.g., Fulle et al. 2015; Rotundi et al. 2015; Hilchenbach et al. 2016; Mannel et al. 2016).

Further experiments and computations with millimeter-sized fluffy aggregates will be needed to draw some conclusions about the fluffy/compact nature of such large dust grains. Polarization laboratory measurements and observations also appear to be a good diagnostic tool for retrieving the nature of such dust grains, since light is on average scattered more within compact particles decreasing the degree of linear polarization (Xing & Hanner 1997). The measured phase functions will be freely available in digital form in the Amsterdam–Granada light scattering database (<http://www.iaa.es/scattering>) under request of citation of Muñoz et al. (2012) and this paper.

Comments of an anonymous referee on an earlier version of this paper are gratefully acknowledged. We are indebted to Rocío Márquez from the Scientific Instrumentation center of the University of Granada for providing the SEM images. This work been supported by the Plan Nacional de Astronomía y Astrofísica contracts AYA2015-67152-R and AYA2015-71975-REDT.

ORCID iDs

O. Muñoz  <https://orcid.org/0000-0002-5138-3932>
 F. Moreno  <https://orcid.org/0000-0003-0670-356X>
 J. Escobar-Cerezo  <https://orcid.org/0000-0003-0432-4443>

References

- Acke, B., Min, M., Dominik, C., et al. 2012, *A&A*, 540, A125
 Andrews, S. M., & Williams, J. P. 2005, *ApJ*, 631, 1134
 Ball, J. G. C., Reed, B. E., Grainger, R. G., et al. 2015, *JGR*, 120, 7747
 Bertini, I., Thomas, N., & Barbieri, C. 2007, *A&A*, 461, 351
 Canovas, H., Caceres, C., Schreiber, M. A., et al. 2016, *MNRAS*, 458, L29
 Canovas, H., Schreiber, M. R., Caceres, C., et al. 2015, *ApJ*, 805, 21
 Dabrowska, D. D., Muñoz, O., Moreno, F., et al. 2015, *Icar*, 250, 83
 Dorschner, J., Begemann, B., Henning, Th., et al. 1995, *A&A*, 300, 503
 Escobar-Cerezo, J., Palmer, C., Muñoz, O., et al. 2017, *ApJ*, 838, 74
 Fulle, M., Della Corte, V., Rotundi, A., et al. 2015, *ApJL*, 802, L12
 Hilchenbach, M., Kissel, J., Langevin, Y., et al. 2016, *ApJL*, 816, L32
 Hovenier, J. W., van der Mee, C. V. M., & Domke, H. 2004, Transfer of Polarized Light in Planetary Atmospheres: Basic Concepts and Practical Methods (Dordrecht/Berlin: Kluwer/Springer)
 Kalas, P., Graham, J. R., & Clampin, M. 2005, *Natur*, 435, 1067
 Kataoka, A., Tsukagoshi, T., Momose, M., et al. 2016, *ApJL*, 831, L12
 Kim, S. H., & Martin, P. G. 1995, *ApJ*, 444, 293
 Klein, C., & Hurlbust, Jr. 1993, Manual of Mineralogy (New York: Wiley)
 Laan, E. C., Volten, H., Muñoz, O., et al. 2009, *Icar*, 119, 219
 Le Bouquin, J. B., Absil, O., Benisty, M., et al. 2009, *A&A*, 498, L41
 Lindqvist, H., Nousiainen, T., Zubko, E., et al. 2011, *JQSR*, 112, 1871
 Mackwoski, D. W., & Mishechenko, M. I. 2011, *JQSR*, 112, 2182
 Mannel, T., Bentley, M. S., Schmied, R., et al. 2016, *MNRAS*, 462, S304
 Milli, J., Vigan, A., Mouillet, D., et al. 2017, *A&A*, 599, A108
 Min, M., Hovenier, J. W., & de Koter, A. 2005, *A&A*, 432, 909
 Min, M., Kama, M., Dominik, C., & Waters, L. B. F. M. 2010, *A&A*, 509, L6
 Min, M., Rab, Ch., Woitke, P., et al. 2016, *A&A*, 585, A13
 Mischenko, M. I., & Liu, L. 2007, *JQSR*, 106, 616
 Mischenko, M. I., Travis, L. D., Kahn, R. A., & West, R. A. 1997, *JGR*, 102, 13543
 Mischenko, M. I., & Yurkin, M. A. 2017, *OptL*, 42, 494
 Moreno, F., Muñoz, O., Guirado, D., et al. 2007, *JQSR*, 106, 348
 Muñoz, O., Moreno, F., Guirado, D., et al. 2010, *JQSR*, 111, 187
 Muñoz, O., Moreno, F., Guirado, D., et al. 2011, *JQSR*, 113, 565

- Muñoz, O., Moreno, F., Guirado, D., et al. 2012, [JQSRT](#), **113**, 565
- Muñoz, O., Volten, H., Hovenier, J. W., et al. 2007, [JGR](#), **112**, D13215
- Nousiainen, T., Muñoz, O., Lindqvist, H., et al. 2011, [JQSRT](#), **112**, 420
- Okada, Y., Mann, I., Mukai, T., et al. 2008, [JQSRT](#), **109**, 2613
- Rages, K., & Pollack, J. B. 1983, [JGR](#), **88**, 8721
- Riley, C. M., Rose, W. I., & Bluth, G. J. S. 2003, [JGR](#), **108**, 2504
- Rotundi, A., Sierks, H., Della Corte, V., et al. 2015, [Sci](#), **347**, aaa3905
- Tomasko, M. G., Doose, L. R., Lemmon, M., et al. 1999, [JGR](#), **104**, 898
- van de Hulst, H. C. 1957, *Light Scattering by Small Particles* (New York: Wiley)
- Volten, H., Muñoz, O., Brucato, J. R., et al. 2006, [JQSRT](#), **100**, 429
- Volten, H., Muñoz, O., Hovenier, J. W., et al. 2007, [A&A](#), **470**, 377
- Weinberger, A. J., Becklin, E. E., Schneider, G., et al. 1999, [A&A](#), **525**, L53
- West, R. A. 1991, [Icar](#), **41**, 278
- Wolff, M. J., Clancy, R., Goguen, J. D., et al. 2010, [Icar](#), **208**, 143
- Xing, A., & Hanner, M. S. 1997, [A&A](#), **324**, 805